2022 IEEE/RSJ International Conference on Intelligent Robots and Systems (IROS)
October 23-27, 2022, Kyoto, Japan

Three-Dimensional Dynamic Running with a Point-Foot Biped based on Differentially Flat SLIP

Zejun Hong, Hua Chen and Wei Zhang

***Abstract*— This paper presents a novel framework for point-foot biped running in three-dimensional space. The proposed approach generates center of mass (CoM) reference trajectories based on a differentially flat spring-loaded inverted pendulum (SLIP) model. A foothold planner is used to select touch down location that renders optimal CoM trajectory for upcoming step in real time. Dynamically feasible trajectories of CoM and orientation are subsequently generated by a simplified single rigid body (SRB) model based model predictive control (MPC). A task-space controller is then applied online to compute whole-body joint torques which embeds these target dynamics into the robot. The proposed approach is evaluated on physical simulation of a 12 degree-of-freedom (DoF), $7.95\,\mathrm{kg}$ point-foot bipedal robot. The robot achieves stable running at at varying speeds with maximum value of $1.1\,\mathrm{m/s}$. The proposed scheme is shown to be able to reject vertical disturbances of $8\,\mathrm{N}\cdot\mathrm{s}$ and lateral disturbance of $6.5\,\mathrm{N}\cdot\mathrm{s}$ applied at the robot base.**

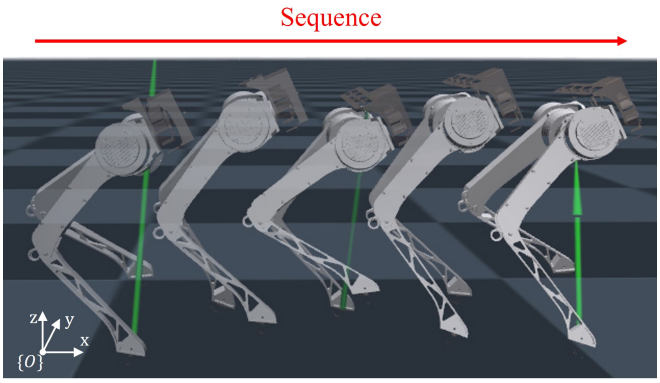

Fig. 1: Snapshots of point-foot bipedal running in the simulation

I. Introduction

Legged robots have attracted considerably rich research and commercial interests recently, owing to their outstanding ability of traversing complex terrains as compared with conventional wheeled robots. Biped robots, which form one of the most important classes of legged robots, have similar work space as human and therefore possess great potentials in various real-world application. However, due to the highly underactuated nature of biped locomotion, the hardware design as well as the control design of biped robot is much more challenging as compared with other sub-classes of legged robots such as quadrupeds.

Apart from test platforms operating in 2D, most biped robots are designed to have actuated or passive soles [1]–[4], which allows for modulating the six-dimensional contact wrench through actuation that are critical for achieving 3D bipedal locomotion. Design of locomotion controllers for biped robots with soles has been investigated extensively in the community. Besides popular zero moment point (ZMP) [5], [6] and capture point [7] based strategies, control schemes for highly dynamic locomotion such as running [8], hopping [9] and long jumping [10] were also carried out by utilizing spring-loaded inverted pendulum (SLIP) model.

This work was supported in part by National Natural Science Foundation of China under Grant No. 62073159 and Grant No. 62003155, in part by the Shenzhen Science and Technology Program under Grant No. JCYJ20200109141601708, and in part by the Science, Technology and Innovation Commission of Shenzhen Municipality under grant no. ZDSYS20200811143601004.

The authors are with Shenzhen Key Laboratory of Biomimetic Robotics and Intelligent Systems, Southern University of Science and Technology, Shenzhen, 518055, China; and with the Department of Mechanical and Energy Engineering, Southern University of Science and Technology, Shenzhen, 518055, China. Emails: hongzj@mail.sustech.edu.cn, chenh6@sustech.edu.cn, zhangw3@sustech.edu.cn

Having a point-foot brings lower swing leg inertia and simpler contact modeling, but induces difficulties in locomotion control due to the reduction of actuated degree of freedom (DoF) in contact. Thanks to the additional DoF introduced by the quadrupedal locomotion features, most quadruped robots adopt the point-foot design and accomplish dynamic locomotion with various schemes, such as virtual model control [11], convex model predictive control (MPC) [12] and variational-based optimal control [13], among others. Inspired by the successfully achieved locomotion with point-foot quadruped, a point-foot biped robot that fully utilizes the power of actuation units is designed as a platform to develop advanced control schemes for highly underactuated locomotion in 3D. As shown in Fig.1, the robot has light-weight mechanical structure and sphere shaped feet whose contact surface with the environment is negligibly small. To release the restriction of motion in a 2D plane, an ab/ad joint is designed at the hip of each leg.

Currently, few successful implementation of 3D locomotion with point-foot biped robot is reported. By deploying prismatic inverted pendulum (PIP) model based CoM trajectory optimization and whole-body control, Hume [14] can balance in simulation and keep upright for 15 steps in physical robot. This approach is hard to be extended to running, since the PIP model remains in contact throughout a motion and can't capture flight phases that are present during a dynamical run. Besides balancing, 3D hopping is achieved with Mini Cheetah [15] in bipedal configuration, in which a SLIP model based CoM trajectory optimization and a control-Lyapunov function based quadratic programming (CLF-QP) tracking controller is applied. This paper studies the problem of 3D running with a point-foot biped robot. Compared to hopping,

2022 IEEE/RSJ International Conference on Intelligent Robots and Systems (IROS) | 978-1-6654-7927-1/22/$31.00 ©2022 IEEE | DOI: 10.1109/IROS47612.2022.9981516

bipedal running is more challenging due to less actuated DoF in stance phase and severer orientation fluctuation caused by asymmetrically switched contacts. Consequently, the underactuation and coupled nonlinear dynamics need to be explicitly considered in control framework along with the hybrid nature of running dynamics, which also motivates the work herein.

A hierarchical architecture for point-foot bipedal running is proposed in this paper, the block diagram is shown in Fig. 2. For desired running speed and apex height, the deployed differentially flat SLIP model based stance planner generates CoM trajectory reference in sagittal plane. The foothold planner selects touch down locations where minimal efforts are required to achieve target take off states. By solving a simplified single rigid body (SRB) model based predictive control problem, the reference base motion trajectory as well as the ground reaction forces (GRF) in 3D are obtained. Given base motion task and foot swing task, the task-space controller is then capable to reproduce the target dynamics through torque control of the biped robot.

II. Planning for Center of Mass and Footholds

Feasible CoM trajectory and footholds that are compatible with each other play a fundamental role in producing stable running motions of point-foot biped robot. The focus of this work is mainly on the motion on the sagittal plane, which dominates the whole-body dynamics in forward running. For online rapid CoM trajectory generation, a 2-dimensional actuated spring loaded inverted pendulum (SLIP) model which captures dominant dynamics of the complex high dimensional multi-rigid body robot model in sagittal plane is deployed for CoM trajectory optimization. Based on the CoM trajectory optimization scheme, proper footholds can be selected.

A. Actuated Spring Loaded Inverted Pendulum Model

An actuated SLIP model with two actuators [16] is considered for CoM trajectory planning. The first actuator can actively adjust the spring length and the second actuator can generate hip torque. Similar to the conventional passive SLIP model, flight phases and stance phases are contained in the actuated SLIP model.

Let $(x, z) \in \mathbb{R}^2$ be the Cartesian coordinates of CoM in a fixed world frame attached at ground, θ be the angle between the positive x axis and leg measured counterclockwise. And the displacement of the linear actuator and the torque given by the rotary actuator are represented as u_1 and u_2, respectively. The equations of motion in stance phase can be written as

$$m\ddot{x} = \frac{kx}{\sqrt{x^2+z^2}}(l_0 - \sqrt{x^2+z^2} + u_1) - \frac{zu_2}{x^2+z^2} \quad (1a)$$

$$m\ddot{z} = \frac{kz}{\sqrt{x^2+z^2}}(l_0 - \sqrt{x^2+z^2} + u_1) - \frac{xu_2}{x^2+z^2} \quad (1b)$$

In flight phase, the massless leg of SLIP model has no dynamical effects on CoM, rendering the following equations of motion

$$\ddot{x} = 0 \quad (2a)$$

$$\ddot{z} = -g \quad (2b)$$

As shown in (1), the actuated SLIP system in stance phase is nonlinear which complicates the trajectory planning problem. By definition, the above derived fully actuated SLIP system is a differentially flat system, in which any trajectory in the flat output space corresponds to a unique controlled trajectory of the nonlinear original dynamics. By utilizing this property, the trajectory planning problem of the actuated SLIP system can be considered in the flat output space, in which complicated differential constraints are transformed to a simple chain of integrators.

B. Differentially Flat SLIP based CoM Motion Planning

The trajectory planning problem of the differentially flat SLIP system can be formulated as an optimal control problem that aims to achieve desired CoM state while respecting all constraints. By taking advantage of the differential flatness property, the trajectory planning problem can be simplified to be planning of flat outputs, which admits a tractable solution based on quadratic programming.

By parameterizing the flat outputs with the following Nth degree polynomial functions

$$x(t) = \phi_0(t)\alpha, \quad y(t) = \phi_0(t)\beta \quad (3a)$$

$$\phi_0(t) = [1, t, t^2, \ldots, t^N] \quad (3b)$$

where $\phi_0(t)$ is basis of the polynomial parameterization, α and β are vectors of polynomial coefficients, the flat outputs and their derivatives $\boldsymbol{y}(t) = (x, \dot{x}, \ddot{x}, z, \dot{z}, \ddot{z})$ can be written as a linear function of the polynomial coefficients, i.e., $\boldsymbol{y}(t) = \bar{\Phi}(t)\gamma$ with $\gamma = (\alpha, \beta)$. The collective polynomial parameterization basis $\bar{\Phi}(t)$ is given as $\bar{\Phi}(t) = \mathrm{Blkdiag}\{\Phi(t), \Phi(t)\}$ with

$$\Phi(t) = [\phi_0^T(t) \quad \phi_1^T(t) \quad \phi_2^T(t)]^T \quad (4a)$$

$$\phi_1(t) = [0, 1, 2t, \ldots, Nt^{N-1}] \quad (4b)$$

$$\phi_2(t) = [0, 0, 2, \ldots, N(N-1)t^{N-2}]. \quad (4c)$$

Given the algebraic relationships in (1), the flat outputs $\boldsymbol{y}^0$ and $\boldsymbol{y}^{\mathrm{d}}$ associated with given initial condition $(\mathbf{x}^{\mathbf{0}}, \mathbf{u}^{\mathbf{0}})$ and the desired terminal state $\mathbf{x}^{\mathrm{d}}$ can be easily computed.

Based on the above discussion, the trajectory planning problem can be formulated as the following quadratic programming over polynomial coefficients

$$\min_{\gamma} \quad \int_0^T \|\bar{\Phi}(t)\gamma - \boldsymbol{y}^{\mathrm{ref}}(t)\|^2_{\boldsymbol{Q}_1} \mathrm{d}t + \|\bar{\Phi}(T)\eta - \boldsymbol{y}^{\mathrm{d}}\|^2_{\boldsymbol{Q}_2} \quad (5a)$$

$$\text{s.t.} \quad \bar{\Phi}(0)\gamma = \boldsymbol{y}^0, \quad (5b)$$

$$[0, \phi_1(T)]\gamma > 0, \quad [0, \phi_2(T)]\gamma = -g \quad (5c)$$

where $\boldsymbol{y}^{\mathrm{ref}}(t)$ is the nominal trajectory, $\boldsymbol{Q}_1$ and $\boldsymbol{Q}_2$ are weighting matrices that denote running and terminal costs.

It is noted that the penalization in the deviation from $\boldsymbol{y}^{\mathrm{ref}}(\cdot)$ in the above formulation implicitly addresses the state and input constraints that are involved in the differentially flat SLIP system. The related states and inputs are softly constrained through carefully designed $\boldsymbol{y}^{\mathrm{ref}}(\cdot)$, which renders solution that respect all these constraints.

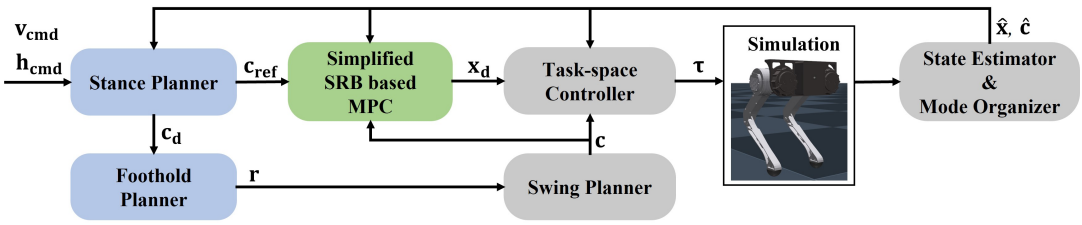

Fig. 2: Proposed bipedal running control architecture. Blocks in blue and block in green are triggered by contact event and run online at 30Hz, blocks in gray run online at 500Hz.

In this problem, $\boldsymbol{y}^{\text{ref}}(\cdot)$ is generated by forward simulating the nonlinear dynamics of (1) starting from the current state $\boldsymbol{y}^0$ with zero input $\mathbf{u}^{\text{ref}}$. The time horizon T of (5) is selected as the instant in which the states of SLIP system satisfies the lift off condition. The resultant trajectory $\boldsymbol{y}^{\text{ref}}(\cdot)$ is then fitted with a polynomial of degree N. By expressing $\boldsymbol{y}^{\text{ref}}(\cdot)$ with the derived polynomial, (5) can be reformulated using a standard quadratic program.

C. Foothold Planning

For pre-defined target lift off state, the value function $V_S(\boldsymbol{y}^0)$ of (5) explicitly represents the quality of touch down state. During the flight phase, since the CoM follows a ballistic trajectory, the touch down state can be uniquely determined when the touch down angle is given. The optimal touch down angle for the upcoming stance phase can then be approximated by the touch down angle whose corresponding touch down state has the minimal value of $V_S(\boldsymbol{y}^0)$.

The leg mass is about 17% of the total mass. Thanks to low leg inertia, the swing motion barely influences the base angular momentum. Furthermore, besides the flight time, the stance time is also available for the swing leg to reach its target position in running motion, which eases the swing velocity requirement, and also in turn reduces the angular momentum effect during flight phase. Therefore, the base motion during flight phase can be well approximated through a ballistic motion. Given this fact, the SLIP model in flight phase also captures the main parts of robot dynamics. The above mentioned optimal touch down angle can be directly interpreted as the location for the next foot touchdown.

Although the concrete optimal touch down location remains unknown during stance phase, the stance time can still be utilized for swing leg to reach a nominal target foothold which renders minimal effort according to the value function of (5) to achieve the desired lift-off states for upcoming stance. During flight phase, the target foothold is then online adjusted according to the instantaneous base states. By applying this strategy, the configuration of swing leg with negligible inertia is able to roughly reach the nominal touch down angle at the lift-off instant even for high-speed running case. Consequently, the variation of leg swing angle during flight phase always remains minor.

D. 3D Implementation with Convex MPC for Simplified SRB Model

Although the differentially flat SLIP model captures the main part of point-foot biped running dynamics, the dynamics in lateral direction is not considered, which is crucial to maintain balance in 3D implementation. Besides, due to highly underactuated features of the robot dynamics and mechanical structure, the coupling between translational and rotational motion is nonnegligible.

To improve the dynamical feasibility of the CoM trajectory reference in sagittal plane and take into account the motion in lateral direction, the CoM and orientation trajectory optimization of robot is conducted based on a simplified SRB model [12] in a receding horizon manner.

SRB model approximates the point-foot biped whole body dynamics through ignoring the inertial effects of both legs, whose equations of motion are given below

$$\ddot{\mathbf{p}} = \frac{1}{m}\sum_{i=1}^{n_c}\mathbf{F}_i - \mathbf{g} \tag{6a}$$

$$\dot{\mathbf{R}} = \boldsymbol{\omega} \times \mathbf{R} \tag{6b}$$

$$\frac{\mathrm{d}}{\mathrm{dt}}(\mathbf{I}\boldsymbol{\omega}) = \sum_{i=1}^{n_c}(\mathbf{c}_i - \mathbf{p}) \times \mathbf{F}_i \tag{6c}$$

where $\mathbf{p} \in \mathbb{R}^3$ denotes the CoM position, m is the robot mass, $\mathbf{F}_i \in \mathbb{R}^3$ is the contact force at the i-th contact point, $\mathbf{g}$ is the gravitational acceleration constant, $\mathbf{R} \in \mathrm{SO}(3)$ is the rotation matrix representing the orientation of the SRB, $\boldsymbol{\omega} \in \mathbb{R}^3$ is the angular velocity of the SRB, $\mathbf{I}$ is the rotational inertia of the SRB, and $\mathbf{c}_i$ is the position of the i-th contact point.

The robot's orientation is described as a vector of Z-Y-X Euler angles $\boldsymbol{\Theta} = (\phi, \theta, \psi)$, where ϕ is the roll angle, θ is the pitch angle, and ψ is the yaw angle. By substituting instantaneous rotation matrix into (6b) and (6c), the above SRB dynamics can be simplified to be a linear time-varying system provided with the CoM reference trajectories and contact references. Discretizing the simplified SRB system with the sampling period δt, the discrete time state space model is given as:

$$\mathbf{x}_{k+1} = \mathbf{A}_k(\boldsymbol{\Theta})\mathbf{x}_k + \mathbf{B}_k(\mathbf{p}_k^{\text{ref}}, \mathbf{c}_{ik}^{\text{ref}}, \boldsymbol{\Theta})\boldsymbol{u}_k + \mathbf{g} \tag{7}$$

where $\mathbf{x}_k = [\boldsymbol{\Theta}_k^T \ \mathbf{p}_k^T \ \boldsymbol{\omega}_k^T \ \dot{\mathbf{p}}_k^T]^T$ is the system state, $\mathbf{u}_k = [\mathbf{F}_{1k}^T \ \mathbf{F}_{2k}^T]^T$ is the control input, $\mathbf{p}_k^{\text{ref}}$ is the reference CoM position, $\mathbf{c}_{ik}^{\text{ref}}$ is the reference position of the i-th contact, the index k denotes the number of time step.

The CoM reference in lateral direction and the orientation is designed to be constant throughout the time horizon of trajectory. Combined with the reference trajectory generated via the previously discussed trajectory optimization scheme,

planning with the simplified SRB model is formulated as the following convex model predictive control problem

$$\min_{\mathbf{x},\mathbf{u}} \quad \sum_{k=0}^{n-1} \|\mathbf{x}_{k+1} - \mathbf{x}_{k+1}^{\text{ref}}\|_{\boldsymbol{Q}_k} + \|\mathbf{u}_k\|_{\boldsymbol{R}_k} \tag{8a}$$

$$\text{s.t.} \quad \mathbf{x}_{k+1} = \mathbf{A}_k\mathbf{x}_k + \mathbf{B}_k\mathbf{u}_k + \mathbf{g} \tag{8b}$$

$$\underline{\mathbf{c}}_k \leq \mathbf{C}_k\mathbf{u}_k \leq \overline{\mathbf{c}}_k \tag{8c}$$

$$\mathbf{D}_k\mathbf{u}_k = 0 \tag{8d}$$

where $\boldsymbol{Q}_k$ and $\boldsymbol{R}_k$ are diagonal positive semidefinite matrices of weights, (8c) corresponds to the friction cone constraint, and (8d) denotes that the GRFs of the legs in swing are zero.

With the proposed planning scheme, reference SRB model state trajectories as well as the GRFs trajectories that are dynamically feasible according to a simplified SRB model are generated. Subsequently, a task space controller is devised to operate the whole robot system.

E. Mode Organizer

A running mode organizer is used to sequence the point-foot biped through phases of stance and flight. The mode organizer has access to the estimated system states $(\hat{\mathbf{q}}, \hat{\dot{\mathbf{q}}})$ in order to detect the transition between different phases. The criteria of lift off (LO) (transition from stance phase to flight phase) is

$$c_{1,z} > 0, c_{2,z} > 0, \dot{p}_z > 0 \tag{9}$$

and the criteria of touch down (TD) (transition from flight phase to stance phase) is

$$c_{i,z} = 0, \dot{p}_z < 0. \tag{10}$$

In LO condition, CoM vertical velocity is additionally required pointing upwards, which prevents the transitioning to flight phase under insufficient kinetic energy of robot system.

III. Task Space Control for Balance and Reference Tracking

Formulating the CoM trajectory, leg swing trajectory and GRFs trajectory as tasks, a task space controller is deployed to compute system torques to track the task dynamics.

A. Tasks Formulation

The whole-body behaviour is authored by characterising the system's desired dynamics in task space. For bipedal running locomotion, tracking the base reference trajectories and leg swing trajectories are main tasks of the controller. Task velocities $\dot{\boldsymbol{x}}_t$ are related to joint angular velocity $\dot{\boldsymbol{q}}$ as

$$\dot{\boldsymbol{x}}_t = \boldsymbol{J}_t(\boldsymbol{q})\dot{\boldsymbol{q}} \tag{11}$$

where $\boldsymbol{J}_t(\boldsymbol{q})$ is a task Jacobian.

The objective of task-space control is to find joint torques $\boldsymbol{\tau}$ that achieve joint accelerations $\ddot{\boldsymbol{q}}$ with

$$\boldsymbol{J}_t(\boldsymbol{q})\ddot{\boldsymbol{q}} + \dot{\boldsymbol{J}}_t(\boldsymbol{q})\dot{\boldsymbol{q}} = \ddot{\boldsymbol{x}}_t \tag{12}$$

such that $\ddot{\boldsymbol{x}}_t$ most closely approach the given commanded task acceleration $\ddot{\boldsymbol{x}}_t^{\text{cmd}}$. The commanded CoM task acceleration $\ddot{\boldsymbol{x}}_{t,CoM}^{\text{cmd}}$ consists of the feedforward CoM acceleration $\ddot{\boldsymbol{x}}_{t,CoM}^{\text{ff}}$ generated by the convex MPC and the feedback terms, which is given as

$$\ddot{\boldsymbol{x}}_{t,CoM}^{\text{cmd}} = \ddot{\boldsymbol{x}}_{t,CoM}^{\text{ff}} + \boldsymbol{K}_{P,CoM}(\mathbf{p} - \mathbf{p}^{\text{ref}}) + \boldsymbol{K}_{D,CoM}(\dot{\mathbf{p}} - \dot{\mathbf{p}}^{\text{ref}}) \tag{13}$$

The leg swing location is regularized by the commanded foot tip acceleration $\ddot{\boldsymbol{x}}_{t,C}^{\text{cmd}}$ computed by

$$\ddot{\boldsymbol{x}}_{t,C}^{\text{cmd}} = \boldsymbol{K}_{P,C}(\mathbf{c} - \mathbf{c}^{\text{ref}}) + \boldsymbol{K}_{D,C}(\dot{\mathbf{c}} - \dot{\mathbf{c}}^{\text{ref}}) \tag{14}$$

B. Constraints Modelling

To account for the dynamical features of the robot system and the interaction with the environment, it is necessary to properly model the constraints for the above task-space control. The dynamic equations of motion of the point-foot biped that are defined as the dynamical constraints are

$$\mathbf{H}(\mathbf{q})\ddot{\mathbf{q}} + \mathbf{C}(\mathbf{q}, \dot{\mathbf{q}}) = \boldsymbol{\tau}_G + \mathbf{S}^T\boldsymbol{\tau} + \boldsymbol{J}_c^T(\mathbf{q})\mathbf{F}, \tag{15}$$

where $\mathbf{q} \in \mathbb{R}^{n+6}$ is the configuration variable of the model containing both the 6 DoF floating base part and all joint configurations, $\boldsymbol{\tau} \in \mathbb{R}^n$ is the input torque command sent to all actuated joints, $\mathbf{F} \in \mathbb{R}^{3\times n_c}$ is a stacked vector containing contact forces at all n_c contacts. $\mathbf{H}(\mathbf{q})$, $\mathbf{C}(\mathbf{q}, \dot{\mathbf{q}})$, $\boldsymbol{\tau}_G$, $\mathbf{S}$ and $\boldsymbol{J}_c(\mathbf{q})$ are the standard generalized inertia matrix, Coriolis and centripetal term, gravitational effect, selection matrix and contact Jacobian respectively.

To maintain foot contact during stance phase, zero accelerations at contact points are enforced to avoid slipping motion, which can be written as

$$\boldsymbol{J}_c(\boldsymbol{q})\ddot{\boldsymbol{q}} + \dot{\boldsymbol{J}}_c(\boldsymbol{q})\dot{\boldsymbol{q}} = \mathbf{0} \tag{16}$$

In the above derivation, all the tasks are predicated on the assumption that given a joint input $\boldsymbol{\tau}$, the ground is capable to supply sufficient forces $\mathbf{F}$ to ensure the contact constraints (16). In fact, the GRFs are limited and the commanded task accelerations should not require GRFs outside their unilateral or frictional boundaries. To this end, the GRFs are constrained by

$$\boldsymbol{W}\boldsymbol{F} \leq 0 \tag{17}$$

where the friction cone is approximated as a friction pyramid and $\boldsymbol{W}$ is the contact constraint matrix.

C. Quadratic Program Formulation of Task Space Control

The task space control problem can be formulated as a quadratic program to determine joint accelerations $\ddot{\boldsymbol{q}}$ and GRFs $\boldsymbol{F}$ that most closely track the commanded task dynamics while satisfying all the constraints. The quadratic program is given blow:

$$\min_{\ddot{\boldsymbol{q}},\mathbf{F}} \quad \|\ddot{\boldsymbol{x}}_{t,CoM} - \ddot{\boldsymbol{x}}_{t,CoM}^{\text{cmd}}\|_{\boldsymbol{Q}_1} + \|\ddot{\boldsymbol{x}}_{t,C} - \ddot{\boldsymbol{x}}_{t,C}^{\text{cmd}}\|_{\boldsymbol{Q}_2} \tag{18a}$$

$$\text{s.t.} \quad \mathbf{H}(\mathbf{q})\ddot{\mathbf{q}} + \mathbf{C}(\mathbf{q}, \dot{\mathbf{q}}) = \boldsymbol{\tau}_G + \mathbf{S}^T\boldsymbol{\tau} + \boldsymbol{J}_c^T(\mathbf{q})\mathbf{F} \tag{18b}$$

$$\boldsymbol{W}\boldsymbol{F} \leq 0 \tag{18c}$$

$$\boldsymbol{J}_c(\boldsymbol{q})\ddot{\boldsymbol{q}} + \dot{\boldsymbol{J}}_c(\boldsymbol{q})\dot{\boldsymbol{q}} = \mathbf{0} \tag{18d}$$

$$\underline{\boldsymbol{\tau}} \leq \boldsymbol{\tau} \leq \overline{\boldsymbol{\tau}} \tag{18e}$$

where $\boldsymbol{Q}_1$ and $\boldsymbol{Q}_2$ express the weights of CoM task and leg swing task, respectively. Joint torques are limited by the

Parameter	Value	Units
m	7.95	kg
I_{xx}	1	$0.1387\,\mathrm{kg}\cdot\mathrm{m}^2$
I_{yy}	1	$0.0891\,\mathrm{kg}\cdot\mathrm{m}^2$
I_{zz}	1	$0.1228\,\mathrm{kg}\cdot\mathrm{m}^2$
μ	0.6	
h_n	0.365	m

TABLE I: Parameters for Point-Foot Biped

Parameter	Value
N	9
$\boldsymbol{Q}_1$	$\mathrm{diag}(1,1,1,1,1,1)$
$\boldsymbol{Q}_2$	$\mathrm{diag}(10^6,10^6,10^6,10^6,10^6,10^6)$
$\boldsymbol{Q}_k$	$\mathrm{diag}(5,10,20,20,20,40,0.1,0.1,0.3,1,1,2)$
$\boldsymbol{R}_k$	$\mathrm{diag}(0.1,0.1,0.5,0.1,0.1,0.5)$

TABLE II: Parameters for Stance Planner and Convex MPC

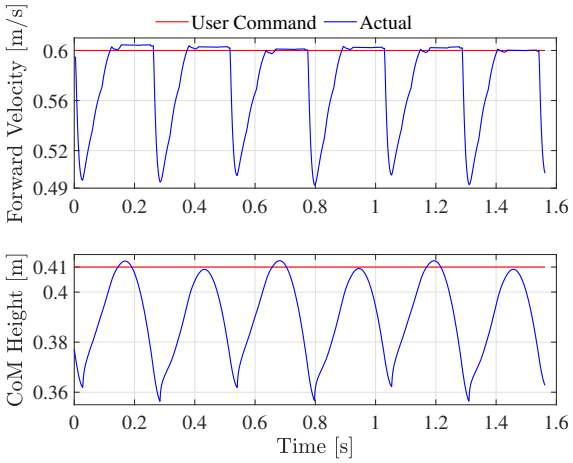

Fig. 3: Forwards velocity and CoM height of robot during running at fixed speed

vectors $\underline{\tau}$ and $\overline{\tau}$, which denotes the bound of deployed actuators' admissible torque. After solving the above optimization problem, the desired joint torques that are sent to the robot can be computed by

$$\boldsymbol{\tau} = (\mathbf{S}^T)^{-1}(\mathbf{H}(\mathbf{q})\ddot{\mathbf{q}}^* + \mathbf{C}(\mathbf{q},\dot{\mathbf{q}}) - \boldsymbol{\tau}_G - \boldsymbol{\Phi}^T(\mathbf{q})\mathbf{F}^*) \quad (19)$$

where $\ddot{\boldsymbol{q}}^*$ are the optimized joint accelerations and $\mathbf{F}^*$ are the optimized GRFs.

IV. Results

The proposed control framework was implemented on a full-body dynamic model of a point-foot biped robot in MuJoCo simulation environment. The point-foot biped robot model has 12 DoF, with 6 actuated DoFs and two point feet. Some of its geometric and dynamics parameters are shown in Table I, where the moment of inertia around each axis is computed at nominal configuration of the robot. The nominal CoM height is denoted by h_n. The weighting matrices for CoM trajectory optimization and convex MPC are given in Table II. By implementing the proposed scheme, the robot is able to achieve stable running with changing commanded speeds and recover from disturbances.

A. Fixed-Speed Running

By giving commanded forward velocity $0.6\,\mathrm{m/s}$ and apex height $0.41\,\mathrm{m}$, stable running with good tracking performance

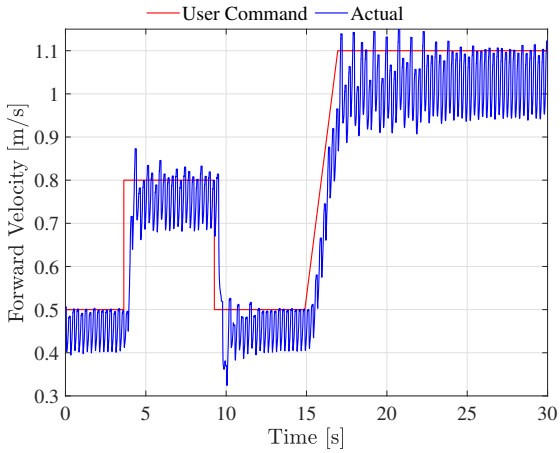

Fig. 4: Command and actual forward velocity

can be achieved with the point-foot biped. Due to orientation variations of robot base during running motion, representing CoM states through base states is inaccurate. Consequently, the forward velocity and CoM height in Fig. 3 are the real CoM states which are computed from estimated robot states. An interval of constant forward velocity occurs in each running step, which interprets the flight phase of running motion. The CoM forward velocity during flight phase and the apex height deviates slightly from the user command, which claims the effectiveness for generating steady-state running motion of the proposed scheme.

B. Speed Variation

Fig. 4 demonstrates the ability to track varying forward velocity command of the proposed scheme. The forward velocity command changes firstly stepwise in a range of $0.3\,\mathrm{m/s}$. The robot can quickly handle these rapid command changes as the steady-state running motion is achieved with commanded CoM forward velocity after a few running steps. A trapezoidal forward velocity reference with constant acceleration of $0.15\,\mathrm{m/s^2}$ is then given to the robot to check its tracking performance. With few lags the robot can follow the velocity reference and achieve stable running motion with the final target velocity.

C. Disturbance Rejection

The online implementation of the motion planning framework enables the robot to effectively handle the unmodeled dynamics as well as the unexpected disturbances. The impacts between the robot and the environment are hard to be modeled and occur frequently due to contact interactions, which result in deterioration of the control performance. As verified before, impacts that happen at contact instant can be well dealt with by implementing the proposed control framework. The capability of recovery from disturbances is then tested by directly changing the velocity of the base link at a specific simulation step, which imitates an ideal impact applied on the robot base. The recovery process after the impact in vertical downward direction with the value of $8\,\mathrm{N}\cdot\mathrm{s}$ is described through the evolution of the forward velocity and

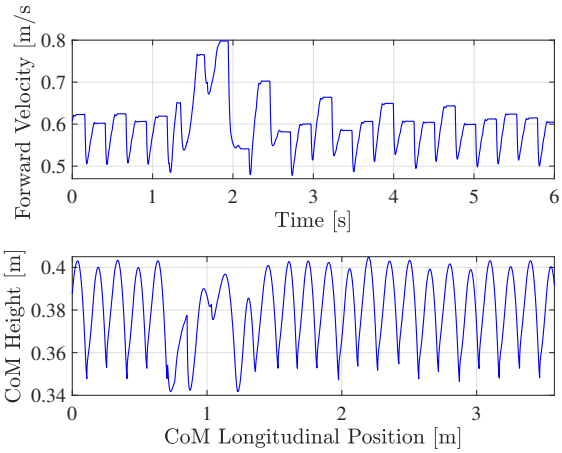

Fig. 5: Evolution of forward velocity and CoM position in sagittal plane near vertical impact instant

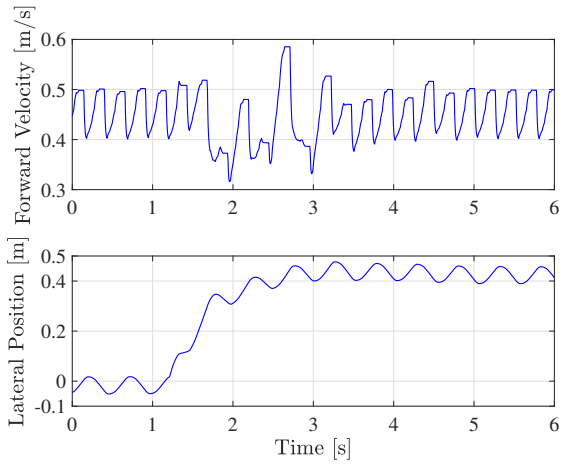

Fig. 6: Evolution of forward velocity and CoM lateral position near lateral impact instant

CoM position in sagittal plane, which are depicted in Fig. 5. Moreover, Fig. 6 represents the forward velocity and lateral position evolution of the robot in response to a sideways push with the value of $6.5\,\mathrm{N}\cdot\mathrm{s}$.

The impact is applied at $1.2\,\mathrm{s}$, at which the robot is in flight phase. Recovering from disturbances that occur in flight phase is more challenging than in stance phase, since there exist no contacts and timely reaction against disturbance can not be conducted. It can be seen that the forward velocity and the CoM position recover to the reference values after suffering several fluctuations, which indicates the robustness of the proposed approach against external disturbances.

V. Conclusions

In this paper, a control framework to achieve 3D running locomotion for point-foot biped robots is proposed. The scheme mainly consists of the planning part and control part. A differentially flat SLIP model based trajectory optimization scheme generates CoM trajectories in sagittal plane. Proper footholds are actively selected during flight phase. The states trajectory of centroidal motions is generated by simplified SRB model based model predictive control scheme. The planned states trajectories are then tracked by a task-space controller. In simulation, the proposed approach enables a point-foot biped robot to achieve 3D stable running at varying speeds. The robustness against external disturbances is also verified through simulation. Future work will consider further behaviors for point-foot biped robots, including experimental implementation on the real hardware.

References

[1] https://www.agilityrobotics.com/cassie.

[2] D. Kim, S. J. Jorgensen, J. Lee, J. Ahn, J. Luo, and L. Sentis, "Dynamic locomotion for passive-ankle biped robots and humanoids using whole-body locomotion control," *The International Journal of Robotics Research*, vol. 39, no. 8, pp. 936–956, 2020.

[3] O. Stasse, T. Flayols, R. Budhiraja, K. Giraud-Esclasse, J. Carpentier, J. Mirabel, A. Del Prete, P. Souères, N. Mansard, F. Lamiraux, *et al.*, "Talos: A new humanoid research platform targeted for industrial applications," in *2017 IEEE-RAS 17th International Conference on Humanoid Robotics (Humanoids)*, pp. 689–695, IEEE, 2017.

[4] K. Kaneko, F. Kanehiro, M. Morisawa, K. Akachi, G. Miyamori, A. Hayashi, and N. Kanehira, "Humanoid robot hrp-4-humanoid robotics platform with lightweight and slim body," in *2011 IEEE/RSJ International Conference on Intelligent Robots and Systems*, pp. 4400–4407, IEEE, 2011.

[5] K. Mitobe, G. Capi, and Y. Nasu, "Control of walking robots based on manipulation of the zero moment point," *Robotica*, vol. 18, no. 6, pp. 651–657, 2000.

[6] S. Kajita, F. Kanehiro, K. Kaneko, K. Fujiwara, K. Harada, K. Yokoi, and H. Hirukawa, "Biped walking pattern generation by using preview control of zero-moment point," in *2003 IEEE International Conference on Robotics and Automation (Cat. No. 03CH37422)*, vol. 2, pp. 1620–1626, IEEE, 2003.

[7] T. Koolen, T. De Boer, J. Rebula, A. Goswami, and J. Pratt, "Capturability-based analysis and control of legged locomotion, part 1: Theory and application to three simple gait models," *The international journal of robotics research*, vol. 31, no. 9, pp. 1094–1113, 2012.

[8] P. M. Wensing and D. E. Orin, "High-speed humanoid running through control with a 3d-slip model," in *2013 IEEE/RSJ International Conference on Intelligent Robots and Systems*, pp. 5134–5140, IEEE, 2013.

[9] P. M. Wensing and D. E. Orin, "Control of humanoid hopping based on a slip model," in *Advances in Mechanisms, Robotics and Design Education and Research*, pp. 265–274, Springer, 2013.

[10] P. M. Wensing and D. E. Orin, "Development of high-span running long jumps for humanoids," in *2014 IEEE International Conference on Robotics and Automation (ICRA)*, pp. 222–227, IEEE, 2014.

[11] M. Focchi, A. Del Prete, I. Havoutis, R. Featherstone, D. G. Caldwell, and C. Semini, "High-slope terrain locomotion for torque-controlled quadruped robots," *Autonomous Robots*, vol. 41, no. 1, pp. 259–272, 2017.

[12] J. Di Carlo, P. M. Wensing, B. Katz, G. Bledt, and S. Kim, "Dynamic locomotion in the mit cheetah 3 through convex model-predictive control," in *2018 IEEE/RSJ International Conference on Intelligent Robots and Systems (IROS)*, pp. 1–9, IEEE, 2018.

[13] M. Chignoli and P. M. Wensing, "Variational-based optimal control of underactuated balancing for dynamic quadrupeds," *IEEE Access*, vol. 8, pp. 49785–49797, 2020.

[14] D. Kim, G. Thomas, and L. Sentis, "A method for dynamically balancing a point foot robot," in *2015 IEEE-RAS 15th International Conference on Humanoid Robots (Humanoids)*, pp. 901–907, 2015.

[15] S. Li, H. Chen, W. Zhang, and P. M. Wensing, "Quadruped robot hopping on two legs," in *2021 IEEE/RSJ International Conference on Intelligent Robots and Systems (IROS)*, pp. 7448–7455, 2021.

[16] H. Chen, P. M. Wensing, and W. Zhang, "Optimal control of a differentially flat two-dimensional spring-loaded inverted pendulum model," *IEEE Robotics and Automation Letters*, vol. 5, no. 2, pp. 307–314, 2019.